



## Research article

# Structural design and material comparison for aircraft wing box beam panel

Peter Korba <sup>a</sup>, Samer Al-Rabeei <sup>a</sup>, Michal Hovanec <sup>a</sup>, Ingrid Sekelová <sup>a</sup>, Utku Kale <sup>b,c,\*</sup>

<sup>a</sup> Department of Aviation Engineering, Faculty of Aeronautics, Technical University of Košice, Rámpová 7, 041 21, Slovak Republic

<sup>b</sup> Department of Aeronautics and Naval Architecture, Faculty of Transportation Engineering and Vehicle Engineering, Budapest University of Technology and Economics, Budapest, Hungary

<sup>c</sup> Aviation Academy, Faculty of Technology, Amsterdam University of Applied Sciences, Amsterdam, the Netherlands

## ARTICLE INFO

**Keywords:**

Wing box beam  
Structural design  
Ansys FEM software

## ABSTRACT

This paper aims to present a comprehensive investigation to obtain the structural calculations needed to design a rigid panel of aluminum alloy for the wing box beam of an ATR 72-500 aircraft. For this design process, several types of materials, including composites like CFRP, are considered so it is possible to compare the actual existing part made of aluminum to them, thus checking the advantages these new materials offer. The research presents an introduction to structural design and provides a study of the relevant literature. The aircraft's principal characteristics and performance abilities were collected so that structural loads can be computed. Research used several methods, a design using conventional methods, applying the theory of elasticity is performed using the Theory of Farrar, allowing us to obtain an analytical solution to the problem, followed by checking the obtained results using Ansys FEM software combined with the parts being designed with CATIA. Furthermore, this same panel is calculated using composite materials instead of conventional aluminum, allowing us to compare both solutions. This research shed light on the intricate process of aircraft structural design, materials selection, and calculation methodologies, highlighting the ongoing pursuit of new and advanced materials. This paper makes clear that using composite materials presents several advantages over traditional ones, allowing for lighter, safer, more fuel-efficient, and more sustainable aircraft. The use of composite materials in the construction of airplane structures is driven by many factors. The results show that the chosen composite materials reduce weight, are durable, have low maintenance requirements, reduce noise, enhance fuel economy, and are resistant to corrosion.

## 1. Introduction

The design of aircraft structures is a complex and challenging task that requires a thorough understanding of the physics and mechanics involved. In particular, calculating the structural properties of rigid panels located in the wing box beam of an aircraft is a real-life problem that design engineers often face during the early stages of aircraft design. This problem requires careful consideration of the aircraft's specific characteristics and the loads the panel will be subjected to.

For over a century, the development of materials for use in aviation has been a key area of focus within the aeronautical industry. From the historic moment when the Wright brothers' airplane made its inaugural flight in 1903, engineers and scientists have been

\* Corresponding author.

E-mail addresses: [kale.utku@kjk.bme.hu](mailto:kale.utku@kjk.bme.hu), [u.kale@hva.nl](mailto:u.kale@hva.nl) (U. Kale).

searching for materials with unique characteristics that can meet the rigorous demands of aviation [1,2]. This has been driven by the need to improve aircraft safety, efficiency, and overall performance. The characteristics that are highly sought after including among others density, mechanical resistance, corrosion resistance, and fatigue resistance.

The first aircraft model was made up of wood and fabric, the first fulfilling a structural role and the second a lifting role. However, due to the characteristics of these materials, they are affected by biological action and do not maintain their properties in all aircraft working conditions (such as humidity) [1]. The wide range of operation that an aircraft must have, oscillating from the 50 °C reached during summer at certain airports to the –60 °C existing on a cruise at 40,000 ft, gave way to the use of metal for structural aeronautical manufacturing. Although steel was the first metal used, this fact led to other problems related to its low corrosion resistance and high-density factors that mean that they are currently only used in specific parts subjected to high loads, such as landing gear [2].

The pursuit of materials that possess these desirable characteristics has been a constant challenge for the aeronautical industry. Materials used in aviation must be able to withstand the high-stress environments that occur during flight, including extreme temperature changes, high-altitude conditions, and exposure to harsh chemicals [3]. Developing new materials that can meet these demands has played a critical role in advancing the aviation industry. It has helped to make air travel safer and more efficient than ever before [4].

Thus, the next stop is to enter into a process of optimization and research in order to find a material that complied with the properties described above and with high specific mechanical resistance, aluminum being the starting point during subsequent decades. Even though aluminum itself does not have good mechanical properties, the use of aluminum alloys adaptable to the aeronautical sector represents a fundamental advance that has covered much of the history of recent aviation. Thus, duralumin arises, which has a higher specific resistance than steel and improves its behavior against corrosion [5].

However, it is necessary to take into account that in addition to the structural function, there are some aircraft components whose main request is thermal resistance. Following this point, precious metal alloys such as tungsten or titanium are used based on their good mechanical strength and thermal properties. The term “superalloys” means alloys that are superior in heat and corrosion resistance and maintain superior properties even at elevated temperatures. Thus, superalloys are synonymous with “high-temperature alloys.” Traditionally, superalloys are classified into three types according to their base element: iron-based, nickel-based, and cobalt-based superalloys [6].

However, in a broader sense, alloys that can preserve their mechanical, physical, and chemical stabilities at high temperatures and in severely corrosive environments are all called superalloys [6]. At room temperature, however, the mechanical properties of superalloys are not much different from steel's, which are much cheaper and quickly produced. However, superalloys stand out from other metallic alloys with their high corrosion resistance even in this temperature range, making them ideal candidates for use in severely corrosive environments such as offshore petroleum platforms [7,8].

Nevertheless, their high cost and the complex process of obtaining and machining that they present mean that these metals are fundamentally limited to some engine parts. Not surprisingly, superalloys' main application area is at elevated temperatures despite impressive room temperature and cryogenic properties [9]. At high temperatures, superalloys are unique in their mechanical and chemical properties [8]. The big leap forward for superalloys was a result of intense effort in developing gas turbine hot section parts to meet the needs of military aircraft. Today, military and civil aircraft gas turbines still play a dominant role in developing superalloys. Aviation gas turbines represent the majority of all applications of superalloys. Among their other application, power-generation gas turbines can be classified, the chemical industry, medical industry, petrochemical equipment, spaceships, rocket engines, nuclear reactors, submarines, high-temperature industrial furnaces, and various other applications that need high-temperature and/or chemical resistance [10–12].

Today, the energy sector strategically plays an even more critical role than ever before because of escalating fuel prices [13]. Global warming and increasing environmental pollution further necessitate more efficient use of petroleum products. The mandate of decreasing fuel consumption and exhaust emissions for aviation and industrial gas turbines is clearly paramount [14]. This dictates the key positioning and new development direction of all superalloys. Therefore, in the current technological context, a compromise solution that maintains properties close to those of aluminum alloys but with a notable decrease in the weight of the structural components has been developed, being the use of composite materials had a fundamental advance during the last years [15].

Composite materials refer to the combination on a macroscopic scale of two or more uniformly distributed materials, being formed by fibers (generally carbon, glass, or Kevlar), which are responsible for supporting most of the loads and providing the pieces with strength and rigidity, and by a matrix (thermosetting or thermoplastic resins) that provide cohesion, hold the fibers together and transmit loads between them [16]. The fact of being able to obtain properties that either of the two constituents cannot achieve independently makes composite materials a versatile solution with a great future in the technological sector.

In addition to weight reduction, which implies a decrease in fuel consumption, lower greenhouse gas emissions, and less operating costs, composite materials have better behavior against impact, corrosion, and abrasion, in addition to high thermal resistance [17]. The evolution of the composite material within the aircraft developed in the last 45 years demonstrates that aircraft such as the B-787 and the A350 (contemporary and competing within the same market segment) currently exceed 50 % of composites [3].

The distribution of materials used in manufacturing the B-787, where there is a preponderance of composite materials compared to metals such as aluminum or steel despite being an aircraft designed 15 years ago. This aircraft is fabricated with more than 50% of composites. Particularly, steel is used in highly requested areas, such as the pylons of both engines [18]. The fact that both Airbus and Boeing, the two leading companies that dominate international aeronautical manufacturing, dedicate significant resources to the optimization of structural design and the development of composite materials shows the current trend within the aeronautical sector.

Another aspect to highlight in the search for innovation in materials and processes to lighten the weight of an aircraft is the use of techniques such as topological optimization and additive manufacturing to manufacture parts that, without necessarily being made of

more advanced materials, are lighter than if they would have manufactured and designed with conventional techniques [19]. This process unfolds, starting from a conventional design to iterating removing material that is not mechanically stressed until a final design with the same mechanical strength but a significantly lower weight. As a result of this development process, the present assignment proposes the structural design of a rigid panel from different points of view. On the one hand, a more traditional design uses aluminum; on the other, a more advanced one uses composite materials. This will allow us to compare the results and be able to draw a justified conclusion on the trend in aircraft structural design and manufacturing [20].

For this research, ATR 72–500 airplane has been chosen as our reference aircraft. This aircraft is widely used throughout Europe as a regional medium-haul transport, and abundant information and data are available on its airframe and structures. Additionally, the ATR 72–500 has a simpler construction compared to other larger aircraft, which means that it is easier to deal with fewer parameters and simpler geometries while still maintaining a rigorous calculation method.

The structural typology of the ATR 72–500 aircraft is semi-monocoque, with a high wing that is structurally a wing box beam type. The wing box beam has two main longitudinal crossbar beams, with the wing upper and lower fairings serving as structural parts. Thus, the aircraft has a square section beam of a variable section, as the outer part of the wing has a decreasing chord, compared to the middle sections, in which the chord is constant. The designed panel is part of the discussed fairing of the wing structure, considering the section at the root wing embedding with the fuselage. This is the weakest point of the structure, with a predominance of bending forces, and the panel must be designed accordingly.

Aluminum would have typically made up an aircraft's main, secondary, and tertiary structure; for many years, metal alloys were seen to represent the pinnacle of technological advancement. However, currently, sophisticated composite materials are preferred for usage in structural aircraft design. To determine the possible use, we conducted a set of measurements in the simulated environment, however, it was not possible to make the measurement and the real environment. This research contributed to the excellence in aerospace and studied the increase of composite materials quality in the aerospace industry. Composite materials can reduce the weight of materials used in the aerospace industry and at the same time increase the efficiency of performance and safety management.

This whole article is organized into several sections. Firstly, the main data and parameters of the reference aircraft are presented. Followed by Section 2, which reviews the current state of the art. In Section 3, our methodology and material selection is described. In this section, current technical solutions employed in aircraft structures and the specific calculation methods used will be discussed, including analytical and FEM techniques. Section 4 provides a step-by-step presentation of the results obtained from the methods employed to calculate the rigid panel. Section 5 presents a discussion of the findings of this article. Finally, Section 6 draws conclusions based on the results obtained.

## 2. Related work

Over the years, the aeronautical sector, in general, and aircraft design, in particular, have experienced substantial growth and technological improvements, leading to techniques used today. However, processes related to maneuver envelope and load calculations are basic elements which have to be obtained for the development of our problem, and others such as using composite material in aircraft design or FEM analysis, are important advantages that have been developed during the last decades.

Although most of the research of the project is related to aircraft structural design, it is necessary to mention the aids used in the software needed for solving the problem. Following this point, it is important to mention reference [21] which is a tutorial of CATIA V5 which outlines the main capabilities and applications of this software, as well as more specific projects like [22], focused on similar works to this paper working with CATIA V5 and Nastran-Patran as computer software for the work of an engineer. Furthermore, FEM calculations have been processed with the student version of ANSYS, employing reference [23], which outlines the most important uses of ANSYS Mechanical APDL for aeronautical structural purposes.

The preliminary design calculations of this paper included the definition of the maneuvering envelope of the ATR-72. According to Ref. [24], it is crucial not to fly in conditions out of this envelope as fatal disasters can occur. Furthermore, reference [25] also used this method to design of a regional turboprop aircraft, and reference [26] discusses the results of diagram n-V. All these considerations are based upon international norms such as CS-25 [27,28] for defining legal prescriptions the aircraft has to meet.

Another important consideration for the dimensioning of the panel is the calculation of loads applied to the wing structure. For this, it is necessary to distinguish between loads described in Ref. [26], such as structural, aerodynamic, engine, and fuel mass. In addition, further contemporary bibliographies have been revised, such as [29], in which a preliminary design of a wing box structure is performed by doing several numerical and CFD load calculations and previously cited [22], where loads are calculated before introducing them in the FEM analysis.

For a deeper understanding of aerospace structural design, a book [30] has been used as a general reference to know common solutions adopted for this purpose. Other specific problems related to structure, such as buckling, are developed in Refs. [31–33]. Different wing box calculation approaches are made by integrating static, buckling, fatigue, and manufacturability requirements and their different loading conditions. Nonetheless, in the above-cited [22] reference, a similar methodology for wing calculations was performed.

However, the cornerstone of this paper is based upon the Theory of Farrar, which was first conceived in 1949 [34] and expanded in 1953 [35] and which considers the design of structural elements subject to mainly compressive loads and having to resist buckling as the main cause of failure. This theory is specifically designed for metal parts and was revised more recently in 2017 [36] with updates regarding computer-aided numerical and FEM considerations.

The second part of the paper is based on the comparison of our solution using aluminum with a composite material approach. In this context, reference [37] has been used as a general-purpose book about aerospace materials, as well as [26,38,39] have been taken as

references for our paper as they are practical studies of the use of composite materials in similar aerostructures.

Other important information regarding the ATR 72 aircraft and its technical and geometrical characteristics could be found in the airplane's manual [40], which is a collection of data and procedures needed to safely operate the aircraft, as well as other sources such as [41–43], where this aircraft gets an in-depth revision as a starting point to design a new similar regional transport airplane. Finally, mathematical models and other important explanations will be presented throughout the paper in corresponding sections.

### 3. Methodology and material

Once the object of the project has been explained and the materials used throughout history in aeronautical structures and the current trends within the sector have been analyzed, this section proceeds to explain the chosen approach and the way to get to the solution of the problem. Fig. 1 shows the process of design and calculation process. Firstly, the analysis of the situation was performed followed by data collection related to the properties of the aircraft in question. Further, the calculation of loads took place in the form of loads due to the structural mass of the wing, loads due to engines, loads due to aerodynamic effects and loads due to fuel tanks. The following simulation permitted the formulation of the results.

The main parameters and characteristics of the ATR 72–500 needed for calculating loads on the airframe are presented in Tables 1 and 2. Table 1 provides information on aircraft components and their masses, as well as key performance parameters and Table 2 offers crucial information on the wing structure and geometry. All this information is critical for accurately determining the loads the aircraft structure must withstand during operation.

Additionally, the necessary assumptions were made about the mass and lift distribution on the wings, the location of the shear center and center of gravity, and the presence of fuel tanks. The assumptions are the following.

- In this research the normally used reference constants have been considered, assuming standard atmosphere (ISA) at sea level ( $\gamma = 1.4$ ,  $R = 287 \text{ J/(kg} \cdot \text{K)}$ ,  $\rho_{SL} = 1.225 \text{ kg/m}^3$ ) and gravity takes the usual value of  $g = 9.8 \text{ m/s}^2$ .
- Mass distribution on wings follows the law  $m(y) = Kc(y)^{1.2}$  and lift distribution is elliptical.
- During cruise flight, lift provided by the wing is 105 % of total aircraft lift, with HTP providing a negative 5 % of it.
- Shear center is located at 50 % of the wing chord, the center of gravity at 40 %, and lift at 25 % of the chord, as it is commonly accepted.
- Two fuel tanks per semi-wing are considered between the aft and stern crossbar beams (at 15 % and 60 % of the chord), with a total fuel amount of 4189.5 L. Further discussion on this topic will be done later.

The commonly used sign criteria for bending moments have been considered throughout the whole research. The objective of this research can be summarized into two main goals. Firstly, the intention is to validate the correctness of the design of a rigid aluminum panel by comparing the analytical results obtained through manual calculations and FEM Ansys software analysis, which permits to simulate and analyze complex load conditions, predict structural behavior and performance, and optimize design variations. Secondly, the aim is to evaluate the feasibility of replacing the conventional aluminum panel with a CFRP composite variant by comparing their respective FEM software calculations.

As part of the analysis, both for the resolution of the metal wing box and the composite material ones, it is essential to analyze the maneuvering envelope for our reference aircraft, obtaining the flight diagram n-V that relates the load factor with the speed of flight. For this, MATLAB programming software will be used. Next, the critical loads suffered by the aircraft in symmetrical steady flight will

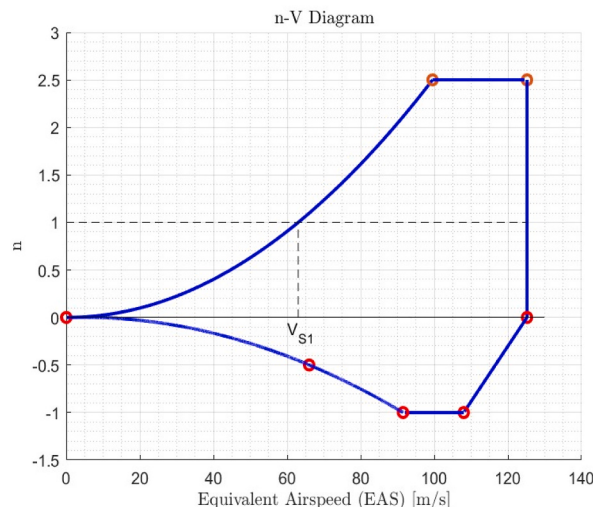


Fig. 1. Flowchart of the design and calculation process.

**Table 1**  
Mass and performance data of ATR 72–500.

Magnitude	Symbol	Value	Units
Maximum Take-Off Weight	MTOW	22800	kg lb
		50625	
Maximum Landing Weight	MLW	22350	kg lb
		49272	
Maximum Zero Fuel Weight	MZFW	20800	kg lb
		45856	
Semi-wing mass	$M_{wing}$	1522.5	kg
Engine mass	$M_{eng}$	887	Kg
Cruise speed	$V_c(TAS)$	140	m/s
Max. negative lift coef. normal to ref. line	$C_{nmax,neg}$	0.715	
Lift coef. normal to ref. line at take-off	$C_{nmax,TO}$	2.145	
Lift coef. normal to ref. line at landing	$C_{nmax,L}$	2.684	
Lift coef. normal to ref. line at landing	$C_{nmax,L}$	2.684	
Lift coef. normal to ref. line clean configuration	$C_{nmax}$	1.511	

**Table 2**  
Wing data of ATR 72–500.

Magnitude	Symbol	Value	Units
Wing surface	$S$	61	m <sup>2</sup>
Chord in the root	$C_r$	2.6	m
Chord in the tip	$C_t$	1.5	m
Span	$b$	27.05	m
Fuselage diameter	$q_{fus}$	2.77	m <sup>2</sup>
Fuselage longitude	$l_{fus}$	27.166	m
One wing longitude	$bow$	12.245	m
Airfoil's center of gravity	$c_{gaf}$	0.4	% C
Airfoil's lift center	$caf$	0.25	% C
Distance between motor's cg and wing leading edge	$x_{eng}$	0.85	m
Distance between motor's cg and wing root	$y_{eng}$	2.665	m

be calculated following the CS 25.333 standard, considering the structural weight of wing and the engines, the aerodynamic loads and the fuel tank loads. During the development, different hypotheses will be carried out that will be discussed throughout the sections. Again, MATLAB programming software has been used for this item, since it is a convenient platform for the numerical calculations and data analysis required for this research, as it was also the case in Refs. [44–46].

Focusing on the design phase, it will be different for both cases. In the case of the aluminum panel, for the analytical calculation, the problem will be approached from the point of view of the Theory of Elasticity and Resistance of Materials, going from loads to tensions and then using the Von Mises criterion to calculate the required thickness of the panel, these were also used in the study [45,47,48]. During the process, the Theory of Farrar, which allows calculating integral panels of metallic materials through the use of an efficiency factor (Farrar's factor) and semi-empirical abacuses, will be used. Mainly, the Theory of Farrar is based on the experimentally demonstrated fact that the optimal design is the one where the torsion of the stringers is negligible and decoupled from the bending of the stringers themselves, thus pure bending being the main mode of the instability of stringers. To quantify this instability, the aforementioned Farrar's coefficient is used. The rest of the elements involved in this theory will be developed in the results section, having once again used MATLAB programming software as the main tool for calculating and developing the iterative process.

This will allow us to get a first approximation of the design which will be helpful in the second stage of the research. During the second stage, the CATIA three-dimensional design software will be used to design the panel and the stringers. At this stage, it is possible to make precise measurements and analysis, by means of this software it allows for testing of different design options and evaluating their impact on the overall structure. Further, the ANSYS structural calculation software will be used to verify numerically if the chosen design is valid, checking the validity of the Theory of Farrar and the behavior of the panel. This stage permits the identification of potential issues with the design and suggestions or modifications to improve strength and stability.

The selection of the right material is crucial as it can significantly affect the aircraft's weight, durability, and overall performance. Therefore, in the final stage of the research, the ANSYS analysis is used to compare the performance of different materials and evaluate the benefits and drawbacks of each material. The ANSYS analysis of a composite material panel is carried out in order to compare the results between both materials. Furthermore, this analysis allows the researchers to validate and support the new trends in materials and manufacturing techniques presented during the related work section.

## 4. Results

### 4.1. Maneuver envelope

In this section, the maneuver envelope is calculated at cruise altitude, computing first of all the limit load factor in accordance with norm CS 25.337, allowing for values between 2.5 and 3.8 and giving a result of the next allowed value of 2.5, as well as  $-1$  for limit negative load factor. On the other hand, dive speed ( $V_D$ ) is calculated after some conversions between Mach number to real speed, obtaining  $V_D = 125.18$  m/s.

Then, maneuver speed is calculated, obtaining  $V_A = 99.51$  m/s. After that, it is necessary to calculate maneuver speed again but for the negative limit load factor, which gives a value of  $V_H = 91.5$  m/s using  $n_{cruise} = 1$ . Then, speed with flaps deployed must be taken into account, using the following formulas and considerations, considering the maximum value among them.

- $1.6V_{S1}$  at MTOW and flaps in take-off configuration.
- $1.8V_{S1}$  at MLW and flaps in approximation configuration.
- $1.8V_{S0}$  at MLW and flaps in landing configuration.

Obtaining a final value of  $V_F = 68.14$  m/s. Finally, as a previous step, before plotting this calculation into the flight envelope diagram, it is necessary to convert from TAS to EAS (true airspeed to equivalent airspeed). Hence, all the results are presented in **Table 3** and in **Fig. 2** as the flight envelope.

### 4.2. Calculation of loads

In this section, the computation of applying loads on the wing box structure will be considered. For this purpose, it is necessary to take into consideration structural weight, the weight of the engines, loads due to aerodynamic effects, and loads due to fuel stored inside the wing tanks. The case of study, according to norm CS 25.333, will be the calculation of critical loads during the stationary symmetric maneuver, given as a result of bending moments, shear and tensile forces, and torque, all for one semi-wing, as there exists a plane of symmetry along the middle of the aircraft.

In following **Fig. 3**, the main dimensions of the wing can be observed, along with the engine's position and the line of torque centers (where it is assumed torque is applied in each section), at 50 % of the chord (hypothesis). Apart from this, it is necessary to determine the exact chord length for each section and the distance between 50 % of chord and a reference straight line for the whole length of the semi-wing, which will be called  $r_{50}$ .

Another hypothesis is that the weight distribution of the wing's structural mass follows this law, with a calculated constant  $K = 42.645$ , obtained from equalling the total mass to the integral of the law along the whole wingspan, see eq. (1).

$$m(y) = K c^{1.2} \quad (1)$$

With all these preliminary calculations being made, it is now possible to start computing and applying loads on the weakest point of the fuselage, which is the embedment of the wing box beam with the main fuselage of the airplane. This is due to the fact that in a cantilever beam, the most significant part of stresses is a result of bending moments accumulating from the tip of the beam to its embedment, something that can be easily extrapolated to our model.

#### • Loads due to the structural mass of the wing

The weight of the semi-wing, which has been considered to be applied at 40 % of the chord for each section of it, is responsible for bending moments ( $M_f$  around the  $x$  axis), torque ( $M_t$  around  $y$  axis) and shear forces ( $V$  in the direction of  $z$  axis). Starting with the calculation of bending moment  $M_f$ , see eq. (2).

$$M_f = -g n_{lim} \int m(y)y dy = -g n_{lim} K \int_{y_{emb}}^{y_{tip}} yc(y)^{1.2} dy = -224706.81 \text{ Nm} \quad (2)$$

Where  $y_{emb}$  is the distance between the middle plane of the aircraft and the embedment at the root of the semi-wing and  $y_{tip}$  is the value of  $y$  coordinate at the tip of the semiwing. The other parameters used have been defined earlier. The negative sign means that the

**Table 3**  
Speed in TAS and EAS (m/s).

Magnitude	VTAS	VEAS
$V_C$	140.70	108.00
$V_D$	163.09	125.18
$V_A$	129.64	99.51
$V_H$	119.20	91.50
$V_F$	68.14	52.30

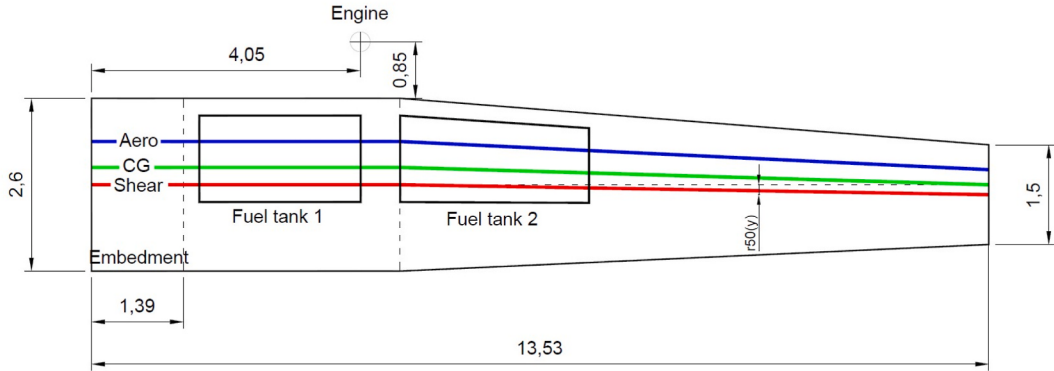


**Fig. 2.** Flight maneuver envelope for ATR 72.

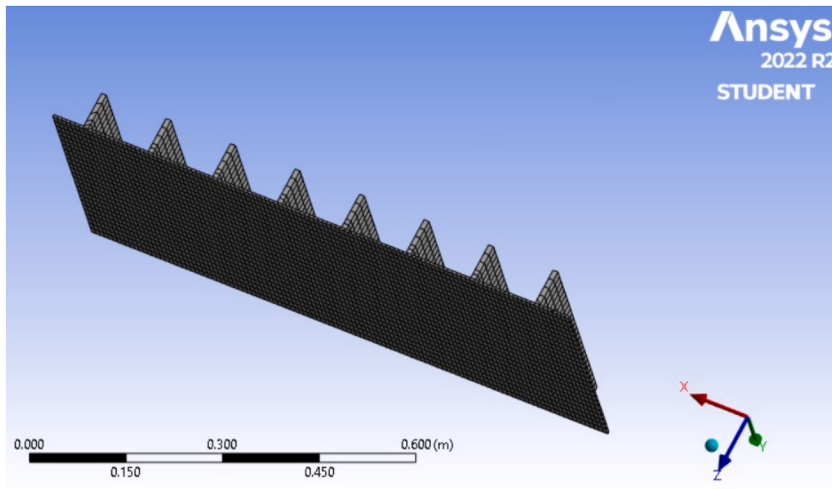


**Fig. 3.** Semi-wing dimensions and hypothesis carried out.

wingtip tends to bend downwards. Then, the torque  $M_t$  can be calculated, which occurs at the embedment of the wing at its root, see eq. (3).

$$M_t = gn_{lim} \int m(y) [ - (x_{tor}(y) - x_{cg}(y)) - r_{50}(y) ] dy = - g n_{lim} K \int_{y_{emb}}^{y_{tip}} c(y)^{1.2} ( - 0.1c(y) - r_{50}(y) ) dy = - 9614.93 \text{ Nm} \quad (3)$$

It can be observed that the order of magnitude of this result is much lower compared to the bending moment and that the negative signs indicate that the whole aircraft would tend to pitch down. This result is in accordance with the fact that the center of gravity line of the wing is located in a more advanced position of the chord than the center of the torque line, where resultants of forces are applied. Finally, the value for the shear force on the critical section of the wing is, see eq. (4).

$$V = - gn_{lim} \int m(y) dy = - gn_{lim} K \int_{y_{emb}}^{y_{tip}} c(y)^{1.2} dy = - 33796.03 \text{ N} \quad (4)$$

This result is nothing more than the vertical force that is caused by the weight of the whole of the structural components of the wing.

#### • Loads due to engines

Now, shear forces, bending moments and torques created by the existence of one engine per wing have to be considered, with a mass of  $m_{eng} = 886.6$  kg each (taking into account all associated systems), and located 4.653 m from the symmetry plane of the aircraft and 85 cm in front of the wing center line. Furthermore, the assumption is made that the engine's mass is concentrated into one point.

With this, calculated bending are in eq (5).

$$M_f = -g n_{lim} m_{eng} y_{eng} = -101173.67 \text{ Nm} \quad (5)$$

Similar comments to the ones made to the loads due to structural mass can be made for this section. Now, the computation of the torque is shown in eq. (6):

$$M_t = g n_{lim} m_{eng} \left( -\frac{c(y_{eng})}{2} + x_{eng} - r_{50}(y_{eng}) \right) = -46749.06 \text{ Nm} \quad (6)$$

Again, it is a torque that induces a pitch down to the aircraft, taking into account the said position of the engines. Finally, shear force on the wing root due to the engine mass can be calculated see in (7).

$$V = -g n_{lim} m_{eng} = -21743.75 \text{ N} \quad (7)$$

#### • Loads due to aerodynamic effects

Another very important source of forces to be taken into account for structural design is aerodynamic forces during flight. Instead of being a force created by opposition to displacement of mass (Newton's Second Law) like in both previous cases, now these are a result of airflow around the wings. A critical hypothesis to consider is that lift can be concentrated for each wing section at 25 % of the chord, an assumption commonly made.

The necessary lift to be provided by the wing is 105 % of the total lift required by the airplane. This is because this type of aircraft is normally designed and trimmed to fly with horizontal tail planes and elevators providing negative lift (5 % of the total). This means that total lift can be calculated as follows, taking into consideration limit load factors and weight of the aircraft, see eq. (8)

$$L = 1.05 n_{lim} MZFW g = 535626 \text{ N} \quad (8)$$

Lift is considered to be elliptical throughout the whole wingspan. As a result, it would be zero at the wingtips and maximum at the center, following this next definition, which gives out the lift for each section of the wing, see eq. (9).

$$l(y) = \frac{4L}{\pi b} \sqrt{1 - \left(\frac{2y}{b}\right)^2} \quad (9)$$

And now, calculation of bending moments, torque, and shear forces can be started. Talking about the bending moment, the following result is obtained in eq. (10).

$$M_f = \int_{y_{emb}}^{y_{tip}} l(y) y \, dy = \int_{y_{emb}}^{y_{tip}} \frac{4L}{\pi b} \sqrt{1 - \left(\frac{2y}{b}\right)^2} y \, dy = 1513179.56 \text{ Nm} \quad (10)$$

Which is positive according to what was expected, which means the wingtips bend upwards as a result of the aerodynamic forces applied on the wing. Torque is calculated following the next two expressions (eqs. (11) and (12)): the first one evaluates the torque created as a result of lift not being applied on the center of the torque line, whereas the second measures torque due to the coefficient of moments  $c_m$ :

$$M_t = \int_{y_{emb}}^{y_{tip}} l(y) [x_{tor}(y) - x_{aero}(y) + r_{50}(y)] \, dy = \int_{y_{emb}}^{y_{tip}} \frac{4L}{\pi b} \sqrt{1 - \left(\frac{2y}{b}\right)^2} (0.25c(y) + r_{50}(y)) \, dy = 148707.04 \text{ Nm} \quad (11)$$

$$M_{t,coeff} = \frac{1}{2} \rho_{SL} V_{EAS}^2 c_m \int_{y_{emb}}^{y_{tip}} c(y)^2 \, dy = -45646.05 \text{ Nm} \quad (12)$$

It has been obtained that both results have different signs, so the first would make the aircraft pitch up (positive) while the second would do the opposite, according to our sign criteria. Moreover, it can be observed that the second value is in absolute value smaller than the first one, so overall torque created by aerodynamic effects makes the airplane pitch up, being of positive value. Finally, shear force can be computed, which is equal to the total lift provided by the wing, see eq. (13)

$$V = L = 535626 \text{ N} \quad (13)$$

#### • Loads due to fuel tanks

The last important item to be taken into consideration to have an estimate of the loads applying to the wing are fuel tanks. According to geometrical considerations on the wing structure, there are two fuel tanks on each semi-wing, with a height of 14 % of total

chord for each section, with the leading part of them at 15 % of chord and the rear at 60 % of the wing, just between the bow and aft main beams of the wing. Furthermore, the length of the first fuel tank goes from 12 % to 30 % of the semi-wingspan, from the embedment of the wing until the engine area, whereas the second one extends from 34.4 % to 89.5 %, taking up part of the volume of the non-constant sections of the semi-wing until reaching the total necessary fuel volume of 4189.5 L.

So, for each tank, it is a requisite to calculate bending moments, torques, and shear forces, considering the positions of their centers of gravity (0.975, 2.840), in m, x, and y coordinates, for the first tank; (1.029, 6.011) for the second. Starting with bending moments in eqs. (14) and (15):

$$M_{f1} = -g n_{lim} V_{ft1} \rho_f (y_{cg1} - y_{emb}) = -29566.23 \text{ Nm} \quad (14)$$

$$M_{f2} = -g n_{lim} V_{ft2} \rho_f (y_{cg2} - y_{emb}) = -95926.48 \text{ Nm} \quad (15)$$

Both bending moments are negative, so they create downward displacement of wingtips. Previously, it has been necessary to compute the volumes of each fuel tank. Torques are calculated in eqs. (16) and (17).

$$M_{t1} = -g n_{lim} V_{ft1} \rho_f (x_{tor}(y_{cg1}) - x_{cg1} - r_{50}(y_{cg1})) = -6604.14 \text{ Nm} \quad (16)$$

$$M_{t2} = -g n_{lim} V_{ft2} \rho_f (x_{tor}(y_{cg2}) - x_{cg2} - r_{50}(y_{cg2})) = -3179.04 \text{ Nm} \quad (17)$$

Where both torques are negative, as their centers of gravity are in a more advanced position compared to the center of torque line of the wing. At last, our last results can be calculated, shear forces as a result of fuel tanks on wings see eqs. (18) and (19).

$$V_1 = -g n_{lim} V_{ft1} \rho_f = -20320.43 \text{ N} \quad (18)$$

$$V_2 = -g n_{lim} V_{ft2} \rho_f = -20736.38 \text{ N} \quad (19)$$

#### • Total loads on critical section

Final results are presented in the following Table 4, and total loads are calculated as the sum of all values for each type of force.

#### 4.3. First case: aluminum panel

Now, structural calculations will be addressed, which will allow to give dimensions to the different elements that make up the wing box of the ATR72, especially the wing panel that has to stand structural loads. Thus, a simple method will be used that comprises the calculation of general parameters of the wing box using classical results of the Theory of Elasticity and Strength of Materials, passing from loads to stresses, both normal and tangential. After that, thicknesses can be computed using Von Mises criterion.

In a second step, Farrar's theory of design of stiffened integral panels will be applied, which are widely used in aviation and are stronger and lighter than those that are reinforced with bolted or screwed small longitudinal beams. The purpose of these beams is to stabilize the panel subject to compression loads to avoid buckling.

Some other important hypotheses and simplifications to be taken into account are that during the preliminary design (before applying Farrar's theory), the panel is modeled as a plain plate of constant width with straight stiffening beams parallel to each other. In the real world, many other requirements must be met, which may not be exactly the case.

##### 4.3.1. Load fluxes calculations and design of wing box

First of all, the calculations needed to design the wing box will be made assuming that it is a monocoque structure with thin walls. This means it will be made up of several panels, comprising upper and lower panels (the ones object of design) and two lateral beams, which in turn make up the wing box structural part.

First of all, it is required to compute inertias, the first of them (cross-inertia) zero due to the symmetric nature of the wing box (a rectangle, with its origin in its center point). Apart from that one, it is also necessary to know  $I_{xx}$ , which is also calculated in the following eqs. (20) and (21):

**Table 4**  
Flight data of ATR 72–500.

Load type	V [N]	$M_f$ [Nm]	$M_t$ [Nm]
Aerodynamic	535626.00	1513179.56	148707.04
$c_m$	–	–	–45646.05
Fuel tank 1	–20320.43	–29566.23	–6604.14
Fuel tank 2	–20736.38	–95926.48	–3179.04
Structural	–33796.03	–224706.81	–9614.93
Engines	–21743.75	–101173.67	–46749.06
<b>Totals</b>	<b>439029.41</b>	<b>1061806.37</b>	<b>36913.81</b>

$$I_{xy} = 0 \quad (20)$$

$$I_{xx} = 2 \cdot \left[ \frac{1}{12} H^3 t_H + L t_L \left( \frac{H}{2} \right)^2 \right] \quad (21)$$

- Normal stresses

The first calculations to pass from loads to stress that can be done is for normal stress  $\sigma$ , which can be computed as follows using the classical formula for computing normal stresses on a section, see eqs. (22) and (23).

$$\sigma = \frac{M_x}{I_{xx}} y = \frac{M_f}{I_{xx}} y \quad (22)$$

$$\sigma_{max} = \pm \frac{M_f}{I_{xx}} \frac{H}{2} \quad (23)$$

- Shear stresses

For shear stresses, it is necessary to compute them both from torque and shear force loads. First of all, torque produces an even distribution of shear stress that can be quantified with the following formula, see eq. (24)

$$q_{0T} = \frac{M_t}{2A} = \frac{M_t}{2HL} \quad (24)$$

On the other hand, shear forces create a shear flux which is given by the expression in eq. (25):

$$q_s = - \frac{S_y}{I_{xx}} \int_0^s t y ds \quad (25)$$

Using some symmetry and anti-symmetry results, the two following equations are obtained, which quantify the flux of shear stresses from the middle of the panel to the upper left corner of the wing box, and from that point to the middle of the left main beam of the wing box, respectively, see eqs. (26) and (27).

$$q_{12} = q_1 - \frac{S_y}{I_{xx}} t_L \frac{H}{2} s \quad (26)$$

$$q_{23} = q_2 - \frac{S_y}{I_{xx}} t_H \left( \frac{H}{2} - \frac{s}{2} \right) s \quad (27)$$

After obtaining the values of shear stresses flux, they can be converted into pure shear stresses by using the following expressions. In them, it is necessary to use the maximum value of shear stress flux and add it to the flux coming from the torque. If the resulting flux is divided by the thickness of the main beams of the wing box, total pure shear stress can be computed, see eqs. (28) and (29).

$$q_{max} = q_{0T} + q_{s,max} \quad (28)$$

$$\tau_{max} = \frac{q_{max}}{t_H} \quad (29)$$

Finally, Von Mises criterion is applied to determine the minimum width that the pair of beams need to have in order to stand the loads obtained before. This is done using an interactive process on MATLAB where thickness is changed until Von Mises criterion converges, see eq. (30).

$$\sqrt{\sigma_{max}^2 + 3\tau_{max}^2} \leq \sigma_e \quad (30)$$

#### 4.3.2. Theory of Farrar

Now, this part will focus on the calculations needed to define all the geometric parameters of the stiffened integral panel. For this purpose, first, it is required to define a safety margin of 50 %, which gives the following results for each of the previously computed loads, see eqs. (31)–(33).

$$M_{f,ult} = 1.5 \cdot M_f = 1592709.56 \text{ Nm} \quad (31)$$

$$M_{t,ult} = 1.5 \cdot M_t = 55390.87 \text{ Nm} \quad (32)$$

$$V_{ult} = 1.5 \cdot V = 658544.12 \text{ N} \quad (33)$$

From the last section, it is necessary to consider shear force and torque fluxes with the same methodology as the one explained before. This results in a shear stress flux of value  $q_B$ . However, it will be needed to calculate a load per unit of length which the panel would have to stand, and that is called  $N_B$ , defining the model with these two parameters.  $N_B$  is now computed in eq. (34).

$$N_B = \frac{M_{f,ult}}{hl} \quad (34)$$

As Farrar's Theory can only work with compressive loads, it is necessary to find a way to transform shear fluxes into an equivalent compressive load, which is called here  $N_{max}$ . In order to do so, a parabolic interaction curve is considered in which normal loads and shear fluxes are correlated after having defined a safety margin ( $q_A$  and  $N_A$  after a 10 % MS definition instead of  $q_B$  and  $N_B$ ). A non-linear equations system can be defined by the next four mathematical expressions in order to obtain  $N_{max}$  see eqs. (35)–(38).

$$\left(\frac{q_A}{q_{max}}\right)^2 + \left(\frac{N_A}{N_{max}}\right)^2 = 1 \quad (35)$$

$$\left(\frac{q_A}{q_{max}}\right)^2 + \left(\frac{N_A}{N_{max}}\right)^2 = (1 + MS)^2 \left[ \left(\frac{q_B}{q_{max}}\right)^2 + \left(\frac{N_B}{N_{max}}\right)^2 \right] \quad (36)$$

$$\frac{q_B}{N_B} = \frac{q_A}{N_A} \quad (37)$$

$$\frac{q_{max}^2}{N_{max}} = \frac{\tau_{max}^2}{F^2(1 + R_b R_t)^2} \frac{L}{E_t} \quad (38)$$

The first of these equations represents the definition of the parabola, while the second one shows the relationship between variables with and without a 10 % security margin ( $q_A$  and  $N_A$  versus  $q_B$  and  $N_B$ ). The third equation is derived from the application of the similarity of triangles and helps to solve the system, whereas the last one shows the relationship between  $q_{max}^2$  and  $N_{max}$  according to Farrar's theory results.

In addition, it is fundamental to define some other parameters necessary for Farrar's design of stiffened integral panel. These parameters are the relationships  $R_b$  and  $R_t$  and Farrar's factor of efficiency  $F$ , shown in the equation below. As it is necessary when in a designing process to maximize efficiency, the optimal values according to theory have been chosen, see eq. (39).

$$R_b = 0.65 \quad R_t = 2.25 \rightarrow F = 0.81 \quad (39)$$

These values are applied on the chart shown in Fig. 5, where entering with  $R_b$  and  $R_t$  values gives out the value of  $F$ . It should be noted that dotted lines represent isolines of the efficiency of the structural part.

Having discussed these values, can now apply them and start obtaining geometric parameters for the stiffening of small beams for the integrated panel. First of all, thickness ( $t_s$ ) can be calculated knowing the thickness of the proper panel, followed by the computing of the width ( $d$ ) from the spacing between beams, see eqs. (40) and (41).

$$t_s = R_t t \quad (40)$$

$$d = R_b b \quad (41)$$

In order to perform  $t$  calculation, the following set of two equations are used, needing as input the distributed load  $N$  applying on the integral panel, see eqs. (42) and (43). Of course, this process is iterative and thus done with the help of MATLAB software until convergence of the whole system is attained.

$$F = \sigma \sqrt{\frac{NL}{E_t}} \quad (42)$$

$$\sigma = \frac{N}{t(1 + R_b R_t)} \quad (43)$$

Combining the last two equations, the final formula is deduced on which a relationship between  $t$  and  $L$ ,  $N$  and  $E_t$  is obtained for the optimal efficiency case of study, see eq. (44).

$$t = \frac{1}{F(1 + R_b R_t)} \sqrt{\frac{NL}{E_t}} \rightarrow t = 0.501 \sqrt{\frac{L}{NE_t}} e \quad (44)$$

Finally, the next set of equations allow for the computing of  $b$  value, which is the spacing between one stiffening beam and the next. These mathematical formulas have been obtained from Farrar's Theory and can be combined for the optimal case in such a way that a straightforward relationship between  $t$  and  $L$ ,  $N$ , and  $E_t$  can be obtained, just like in previous cases see eqs. (45)–(47).

$$\sigma_b = \frac{\sigma_b}{\sigma_0} 3.62 E_t \left(\frac{t}{b}\right)^2 \quad (45)$$

$$F = 1.3136 \left( \frac{\sigma_b}{\sigma_0} \right)^{\frac{1}{4}} \left( \frac{[R_b^3 R_t (4 + R_b R_t)]^{\frac{1}{2}}}{1 + R_b R_t} \right) \quad (46)$$

$$b = 1.103 \frac{\sqrt{F}(1 + R_b R_t)}{[R_b^3 R_t (4 + R_b R_t)]^{\frac{1}{2}}} \left( \frac{NL^3}{E_t} \right)^{\frac{1}{4}} \rightarrow b = 1.33 \left( \frac{NL^3}{E_t} \right)^{\frac{1}{4}} \quad (47)$$

Having already obtained  $b$ , the total amount of stiffening small beams can be computed as the quotient between the width of the panel  $l$  and the spacing of stiffening beams  $b$ , see eq. (48).

$$n_l = \frac{l}{b} \quad (48)$$

Lastly, a value for average stress flowing through the panel is obtained as shown in eq. (49).

$$\sigma_m = F \sqrt{\frac{N_{max} E_t}{L}} \quad (49)$$

Once all these equations are conveniently programmed for the system to be solved with MATLAB, and after doing all the necessary iterations, the following final results in Table 5 for a stiffened integral panel subject to compressive loads are given.

#### 4.3.3. Ansys FEM study

After having calculated analytically the dimensions of the integral panel the dimensions of the integral panel analytically, it is highly advised to perform a FEM analysis (Finite Element Method) to validate these results. For this purpose, a static structural analysis on ANSYS is performed, having defined previously the three-dimensional body on CATIA. This CAD model is then imported into ANSYS, taking the shape that can be seen on Fig. 4, where meshing using a structured pattern has already been implemented (it could have been better if instead of a student license a full one were used, allowing for a finer meshing).

The next step is the definition of boundary conditions and loads. Fixed support has been set as a boundary condition for the embedment on the wing's root, impeding any rotation or displacement. Apart from that, on the lateral faces that stand just above the main beams of the wing box it has been established that our model can only make displacement on the Z directions, whereas on the other face (the one where the load is applied), only displacements along the Y axis are allowed. Regarding the loads, a remote force has been applied evenly over the whole surface of the loaded face after multiplying the value obtained for distributed load  $N_{max}$  by the width of panel  $L$ . All these considerations are shown in Fig. 5.

Another critical definition to be made before any calculations are done is to establish a material. In this case, Aluminum alloy 6061 with thermal treatment T6 has been considered, as it is a widely used material in the aviation industry and particularly common for manufacturing pieces like this integral panel. See Fig. 6.

Once all the parameters of the problem have been defined, now it is turned for the FEM solving of it, giving. As a result, the following pictures, among other things. The first and second ones (Figs. 7 and 8) represent the stress field on the panel, obtaining a maximum stress below the value of yield strength for this material and thus validating previously done calculations.

To complement this stress field, Figs. 9 and 10 show the strain field obtained. Obviously, a high correlation between both fields can be observed, as a more significant stress means the material will suffer from a bigger deformation and, thus, a higher value for strain.

To end up with this FEM analysis and to fully validate results, an eigenvalue buckling analysis is performed on ANSYS, demonstrated in Figs. 11 and 12. This is very important because Farrar's theory is widely based on instabilities that may occur on the panels to define minimum resistance. This means that it would not be uncommon for buckling to happen for a smaller load than for the plasticification of the weakest section.

The most important goal of this buckling analysis is to obtain the load factor in relation to the maximum load considered on a static structural problem for which buckling occurs. If it has a value below one, buckling will happen before the exhaustion of portant capacity on the panel, whereas it would happen above this value for a factor over one. It is interesting to obtain a factor above one but not that much, as that means efficient use of materials. Of course, the factor of around two that has been obtained fully validates all the

**Table 5**  
Results obtained by Farrar's theory.

Magnitude	Value
$N_A$	$2.646 \cdot 10^6 \text{ N/m}$
$qA$	$4.008 \cdot 10^5 \text{ N/m}$
$N_{max}$	$4.578 \cdot 10^6 \text{ N/m}$
$q_{max}$	$6.172 \cdot 10^5 \text{ N/m}$
$\sigma_m$	487.5 MPa
$t$	3.8 mm
$t_s$	7.58 mm
$b$	110.66 mm
$d$	71.92 mm
$n_l$	8

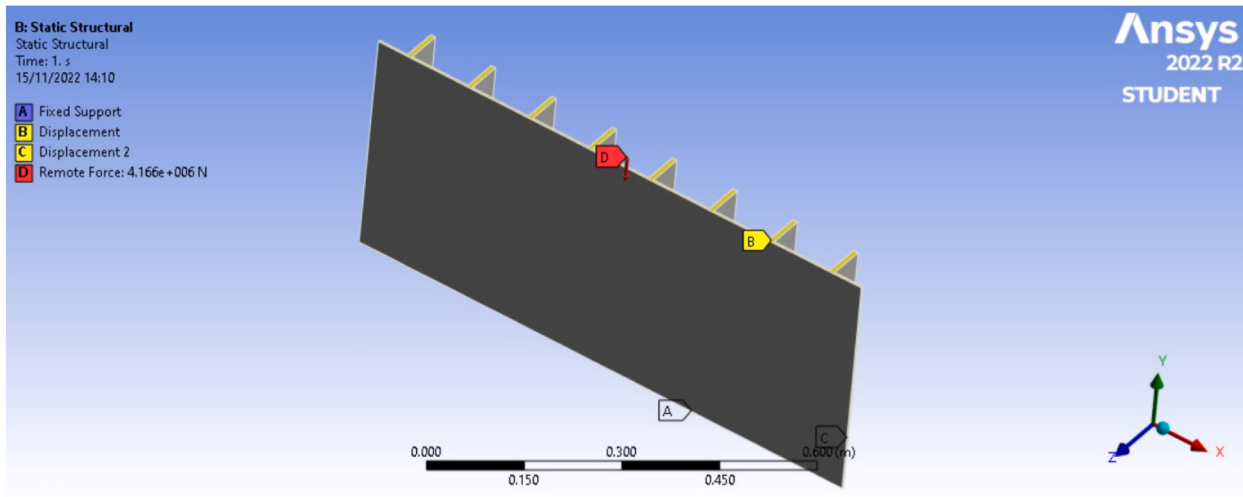


Fig. 4. Mesh generation for FEM analysis with ANSYS.

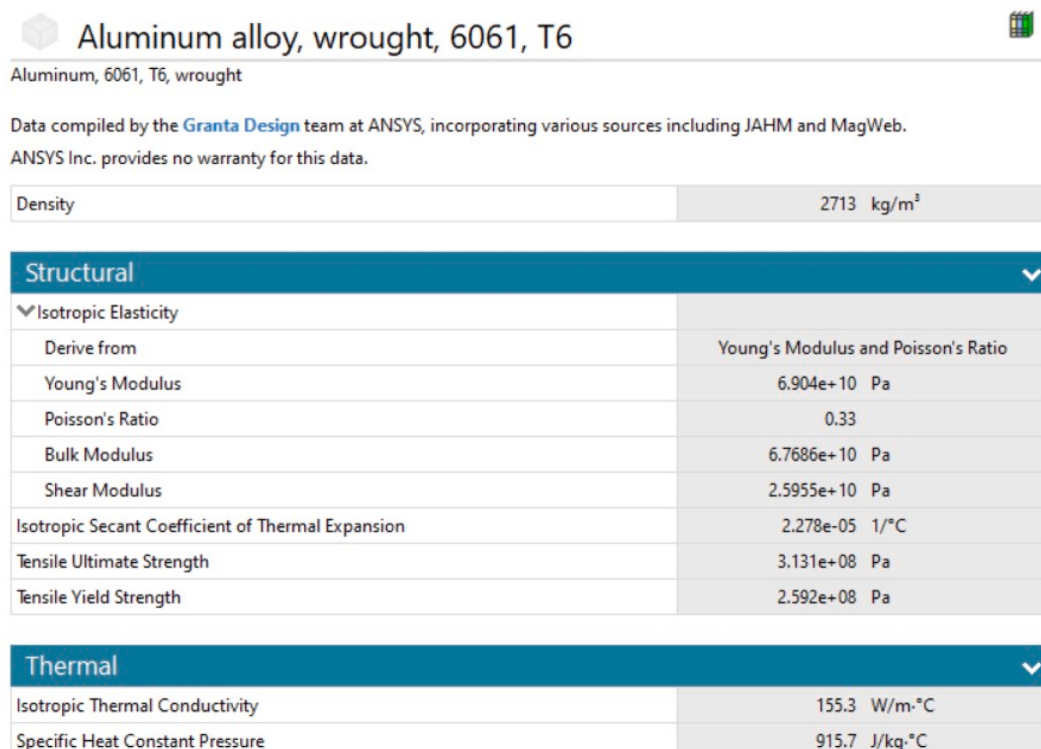


Fig. 5. Boundary conditions and load definition for FEM analysis with ANSYS.

calculations made before.

#### 4.4. Second case: composite material panel

Current trends in material science show that composite materials are advantageous compared to normal ones in many cases. This is due to the fact that composites have a much higher specific strength compared to, for example, aluminum, which makes it ideal for applications where weight saving is paramount, like in aircraft construction.

As presented at the beginning of this article, CFRP (Carbon Fibre Reinforced Composites) is now a widespread material for the

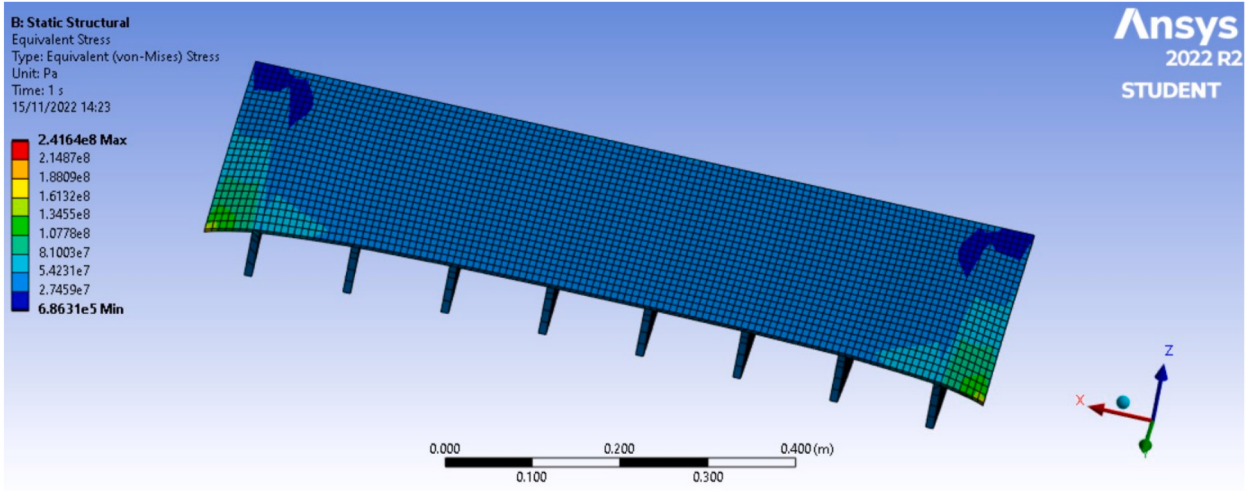


**Fig. 6.** Properties of the aluminum alloy considered as defined in ANSYS.

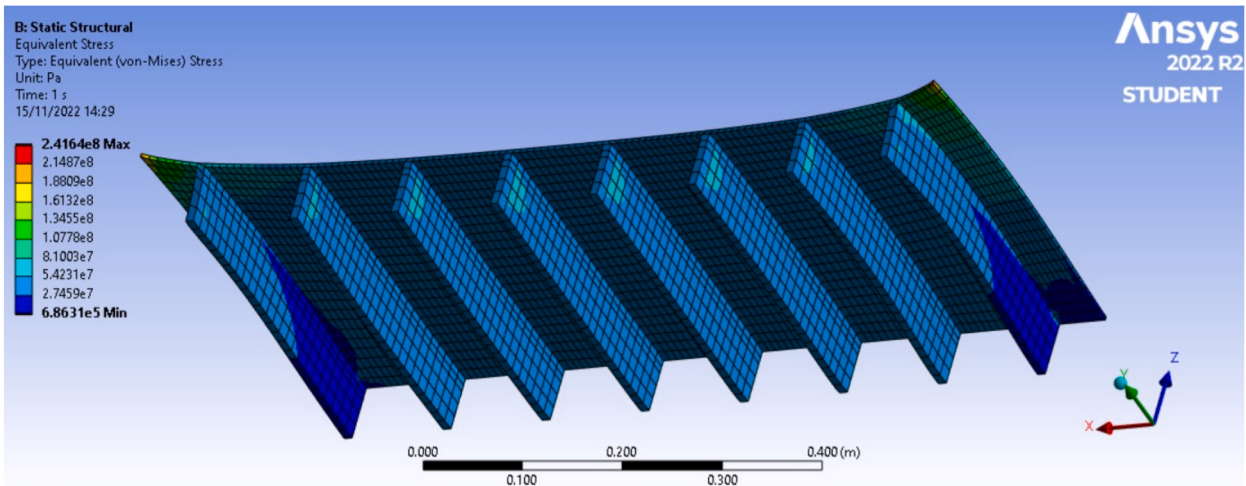


**Fig. 7.** Stress field obtained with FEM analysis with ANSYS (upper part).

construction of airframes and aeronautical structures in general, often comprising more than 50 % in weight of the total structural mass. So, for this study, the same FEM done previously will be implemented but using Epoxy Woven Carbon Fibre prepreg (230 GPa), a commonly used composite on these structures.

Having done the same analysis as with the aluminum panel, the results consist of Fig. 13 showing the stress field, Fig. 14 showing the strain field and Fig. 15 after performing an eigenvalue buckling analysis.

The most interesting thing about this approach with composites is that a factor of about 3 now decreases maximum stress. Consequently, a panel that is not even near to a level of stress that would make it fail but is now lighter than the aluminum counterpart is presented now.

As the density of aluminum is around  $\rho_{Al} = 2700 \text{ kg/m}^3$  and the density of CFRP is about  $\rho_{CFRP} = 1750 \text{ kg/m}^3$ , a 35 % decrease in mass has been attained just by changing from one material to the other. In addition, as CFRP is more resistant than aluminum, further decreases in the thickness of parts could be done, reducing the weight of the part even more (although this analysis is considered to be out of reach for this assignment). As it is known, the weight saving is worth the higher costs of these new materials, which means that analysis such as this one is becoming more common and necessary.

About the eigenvalue buckling analysis, it can be seen that the value of the load factor is higher than in the case of aluminum. This validates all the previous results, as this piece would not be prone to instabilities.

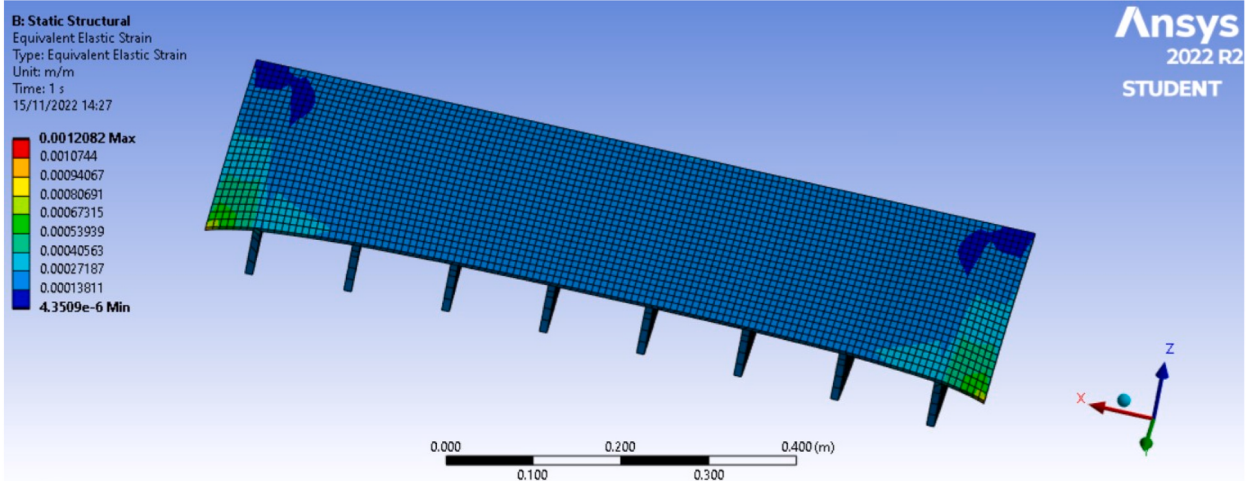


**Fig. 8.** Stress field obtained with FEM analysis with ANSYS (lower part).

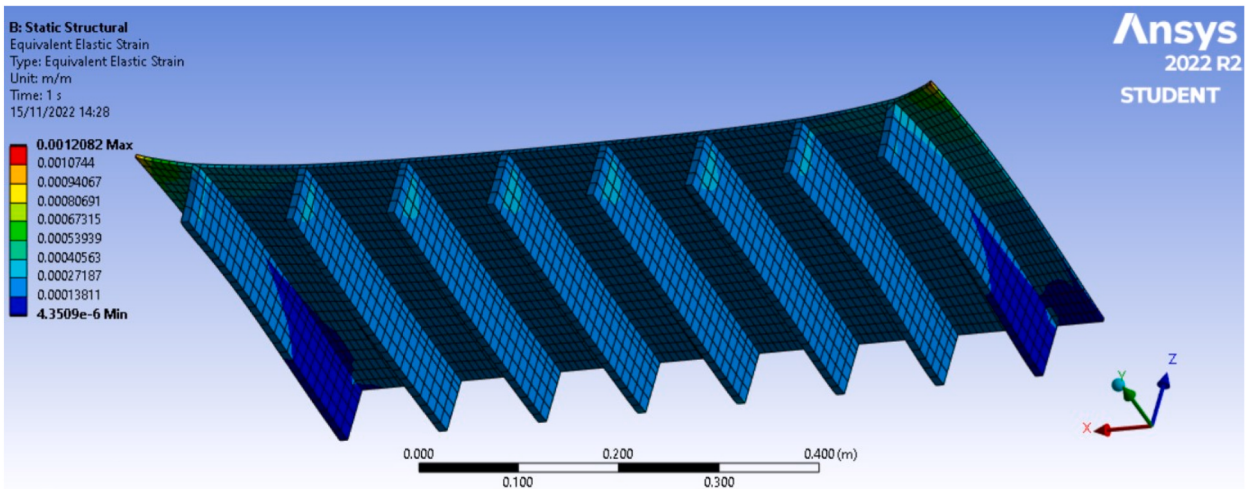


**Fig. 9.** Strain field obtained with FEM analysis with ANSYS (upper part).

## 5. Discussion

The results obtained by the calculations presented in this paper using the Theory of Farrar with the help of MATLAB computing environment for the rigid panel of 91 cm of width for the top or bottom parts of the wing box at its root are the following: 8 stiffening integral beams each with a height of 7.2 cm and a width of 7.6 mm, together with the main panel which is 3.8 mm thick, all made by machining an aluminum piece. With this, an average stress of 487.5 MPa flows through the part mainly due to compressive loads in the critical scenario.

These results were validated using ANSYS Mechanical APDL, where applying boundary conditions and loads were set to match reality as closely as possible, giving values below yield strength for every element of the mesh as well as a critical buckling factor of around 2, which is a good value as it is low enough as to prove that no material is wasted while it is safe enough as buckling would never occur before failure of the part due to plasticification. After that, a similar analysis was performed but now uses CFRP instead of aluminum, which has meant a reduction of mass of around 35 % while retaining good resistance compared to the aluminum part, both in maximum stress and buckling factor.

This last FEM study of the use of CFRP instead of aluminum had some limitations in terms of the definition of the composite, as further work could be done so more precise results could be attained by defining the layer structure of this material. Apart from that, other limitations may also be commented on, such as the definition of loads and boundary conditions for the FEM analysis, as having designed the whole wing structure would have resulted in a more precise solution, something that could be improved in the future.

In terms of the numerical calculations and design phase of the part, some assumptions and the model of the aircraft could be made using a more complex method. However, the authors of this paper believe the one used is appropriate, even though there is always

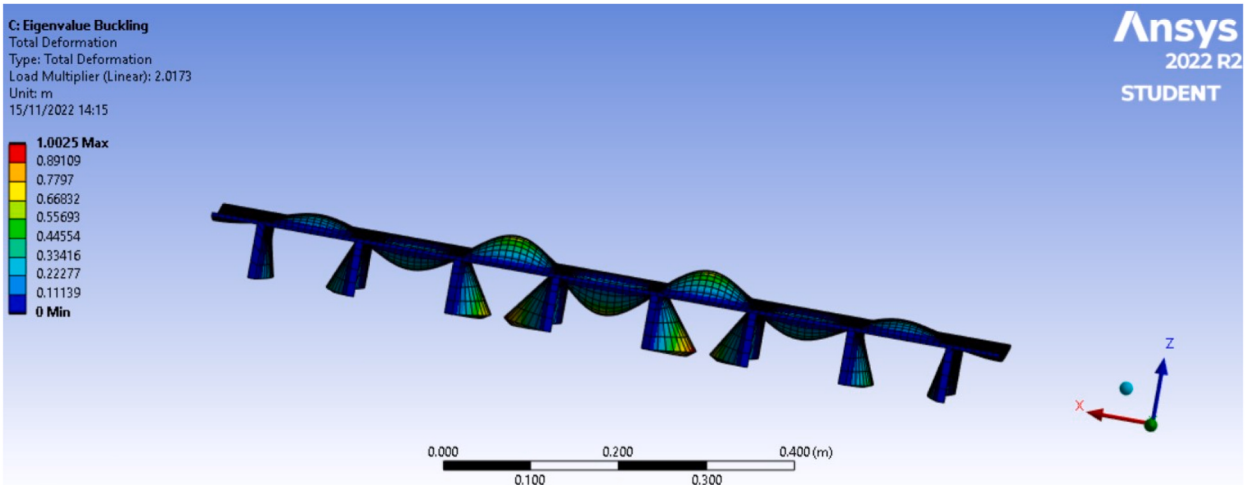


**Fig. 10.** Strain field obtained with FEM analysis with ANSYS (lower part).

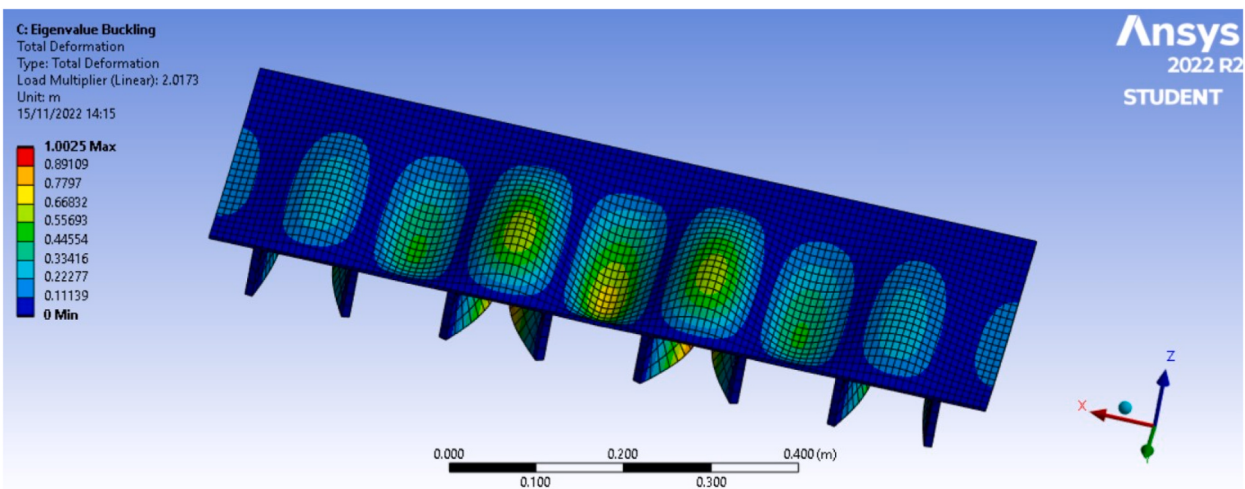


**Fig. 11.** Eigenvalue buckling analysis: strain field due to buckling at critical load (upper part).

some room for improvement. Other minor problems arose when the calculation of the solution using MATLAB was being performed, as some numerical instabilities were detected.

This paper has met the main goals set at the beginning of the research, as the goals of designing and calculating a structural part of an existing aircraft were fulfilled. Furthermore, by comparing the aluminum and CFRP composite parts, it can be acknowledged that the weight reduction these new materials imply over more traditional metallic materials in the aerospace industry and why they are increasingly being used today in practice.

These results may be of high value for other people who want to perform a similar analysis. Even more, any contribution to science that implies the use of novel materials, which eventually means a reduction of greenhouse effect gases, is always beneficial for society, as having a higher volume of scientific work of this kind is a sign that sustainability objectives form the 2030 agenda are in the way of being met.

In comparison with other recent papers, in Ref. [39], a similar problem is studied using comparable techniques, such as the use of CATIA and ANSYS for computer-based analysis of a similar wing structure. Their methodology is very similar, and their results, too, in terms of the advantages that composite materials have to offer, as these present a lower strain level and a reduced weight.

## 6. Conclusion

To conclude, a variety of tools and engineering processes were used in this paper, software like CATIA for CAD, ANSYS for FEM analysis, and MATLAB for calculations, among others, to design via traditional numerical methods and FEM analysis a stiffened rigid panel for the wing box structure of an ATR 72 aircraft. The main objective of the paper is twofold. On the one hand, a real problem has

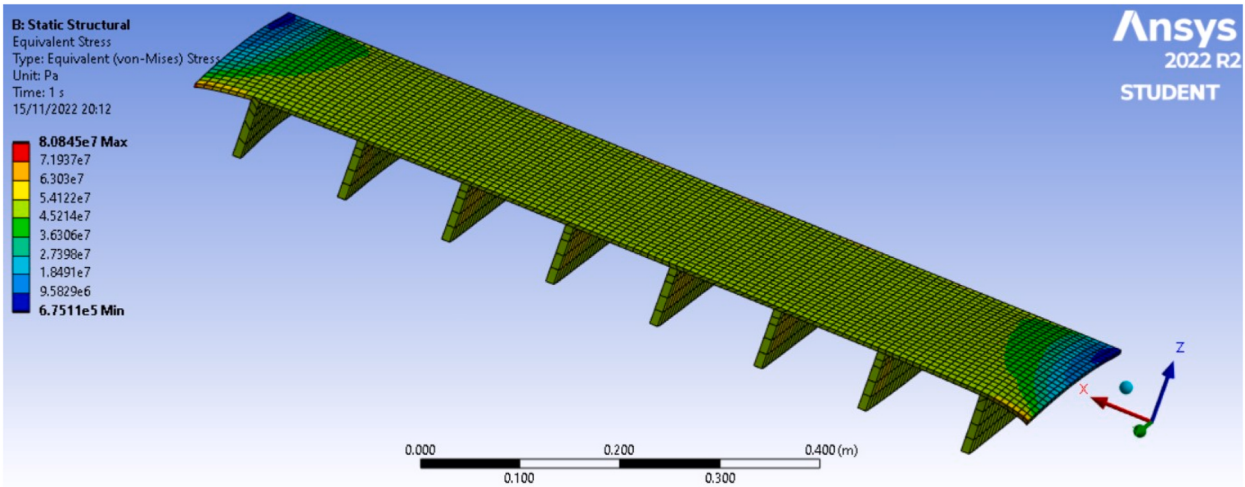


**Fig. 12.** Eigenvalue buckling analysis: strain field due to buckling at critical load (lower part).

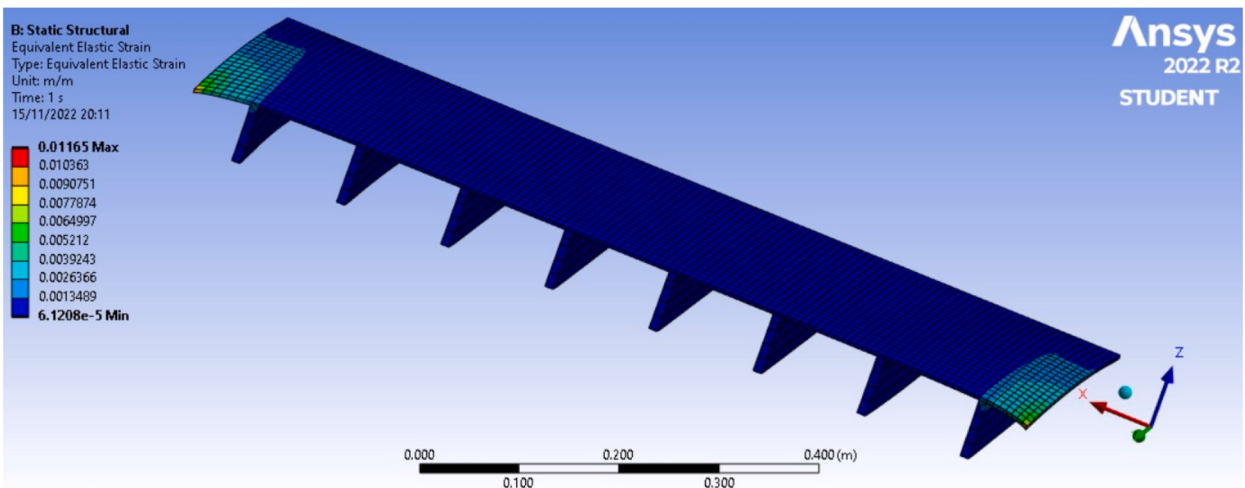


**Fig. 13.** Stress field obtained with FEM on ANSYS for CFRP panel.

been sought that is as close as possible to those an engineer faces in his professional career, having adapted part of the work to the academic field by using some hypothesis explained in each section. On the other hand, the authors used a wide range of tools to achieve a robust solution.

A lot of time has been spent in the research for documents and reference papers and processing this information by the development of equations until some of the expressions shown in this document could be obtained. Also, many very interesting and currently relevant topics in the world of Aeronautical Engineering have been worked on throughout the paper, such as new materials, design optimization, and main techniques for aircraft manufacturing. This paper's main goal was to design a real part for a real airplane, a kind of work commonly performed at enterprises such as Airbus or ATR.

As part of the analysis, the following points have been carefully considered.

- Maneuver envelop of the aircraft and n-V diagram.
- Calculation of loads according to CS 25.333.
- Analytical design according to Farrar's theory.
- 3D design using CATIA V5.
- Implementation and comprehension of FEM analysis results.

Firstly, all the necessary information for the study had to be assembled and studied, and a model for it was established. Then, a maneuver envelope according to CS 25 was conceived, so the critical situations in which the structure of the wings would be under

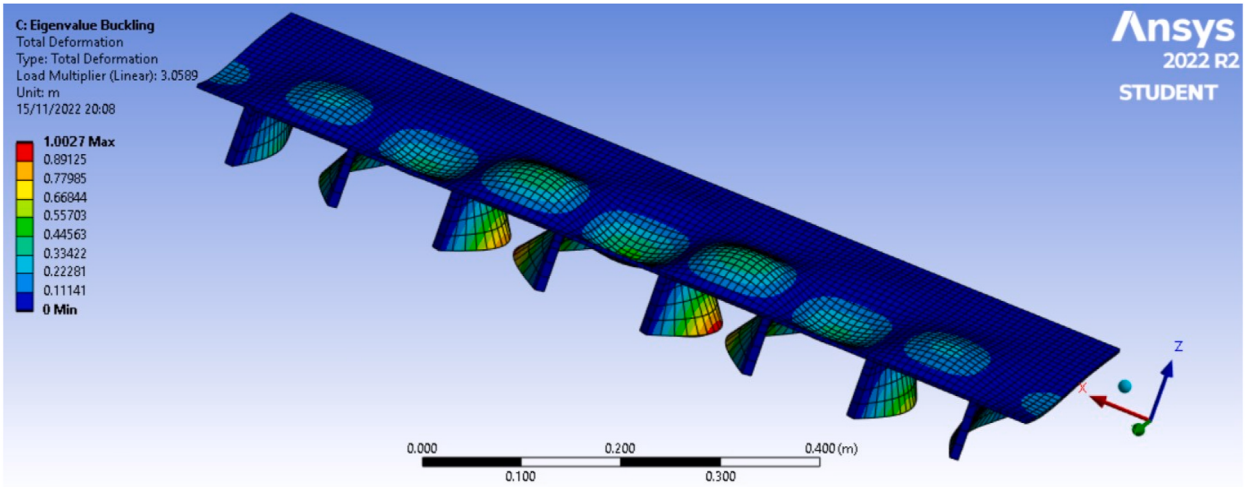


**Fig. 14.** Strain field obtained with FEM on ANSYS for CFRP panel.

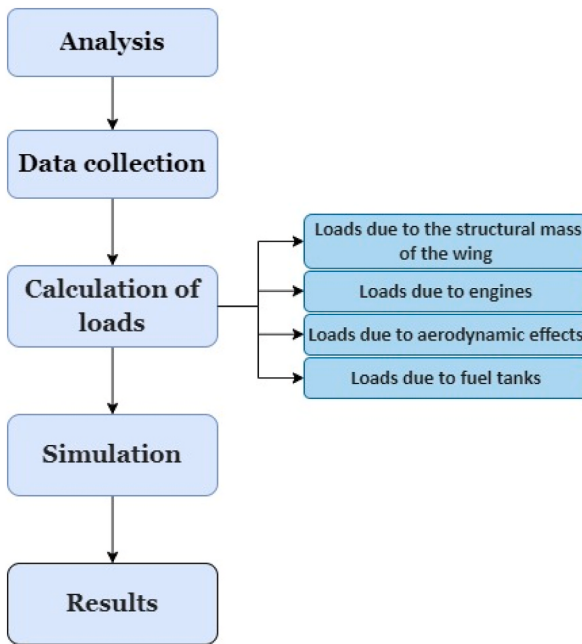


**Fig. 15.** Eigenvalue buckling analysis: strain field due to buckling at critical load for CFRP panel.

higher stress could be defined. With these parameters, it was possible to define the different applying loads according to regulations and the main characteristics of the reference aircraft, obtaining them for the critical section of the wing at the embedment.

Knowing all the structural loads, the Theory of Farrar for the design of stiffened rigid panels was applied, and the geometry and dimensions of this structural part were determined. Further validation of this design was performed by the use of FEM analysis with ANSYS, and a comparison between the designed aluminum panel and an equivalent one made with CFRP composite material, including the weight reduction that these new materials offer compared to traditional ones.

It is simple to see why composite materials are currently preferred over metals in the design and manufacturing of modern aircraft. Although metals will always be used and, in certain cases, cannot be completely replaced by composites, composites provide a range of design options that metal technologies alone cannot match.

The composites industry seems to have a bright future ahead of it, it is expected to improve and ensure sustained long-term growth, and there are always more innovative and newer, exciting products and applications on the horizon.

Furthermore, this paper can help to get a deeper insight into the topic of aircraft structural calculations and design as well as to validate the growing trend in the use of composite materials and their comparison with more traditional materials such as aluminum,

which has been carried out, allowing us to verify the versatility that composite materials offer and the great advantages they entail in terms of weight reduction and increased specific resistance.

## Data availability statement

Data will be made available on request.

## CRediT authorship contribution statement

**Peter Korba:** Writing – review & editing, Supervision, Investigation, Conceptualization. **Samer Al-Rabeei:** Writing – review & editing, Writing – original draft, Validation, Project administration, Methodology, Investigation, Formal analysis, Data curation, Conceptualization. **Michal Hovanec:** Writing – review & editing, Visualization, Supervision, Project administration. **Ingrid Sekelová:** Writing – review & editing, Writing – original draft, Project administration, Methodology, Investigation, Formal analysis. **Utku Kale:** Writing – review & editing, Validation, Supervision, Project administration.

## Declaration of competing interest

The authors declare that they have no known competing financial interests or personal relationships that could have appeared to influence the work reported in this paper.

## Acknowledgement

This work was supported by the Slovak Research and Development Agency under the number APVV-20-0546 - Innovative measurement of airspeed of unconventional flying vehicles and within the “Research of an intelligent management logistics system with a focus on monitoring the hygienic safety of the logistics chain” project implemented under contract number 313011BWP9.

This work was also supported by Project No. 2022-2.1.1-NL-2022-00012, which has been implemented with the support provided by the Ministry of Culture and Innovation of Hungary from the National Research, Development and Innovation Fund, financed under the National Laboratories funding scheme.”

## References

- [1] K. Sharma, G. Srinivas, Flying smart: Smart materials used in aviation industry, *Mater. Today Proc.* 27 (1) (2020) 244–250.
- [2] R. Petrescu, R. Aversa, B. Akash, R. Bucinell, J. Corchado, A. Apicella, F. Petrescu, History of aviation - a Short review, *Journal of Aircraft and Spacecraft Technology* 1 (1) (2017) 30–49.
- [3] A. Ghobadi, Common type of Damages in composites and their Inspections, *World journal od Mechanics* 7 (2) (2017) 24–33.
- [4] L. Setlak, R. Kowalik, T. Lusiak, Practical Use of composite materials used in military aircraft, *Materials* 14 (17) (2021).
- [5] H. Yoshida, History of the development of Extra super duralumin and future research issues of Al-Zn-Mg alloys, *Mater. Trans.* 64 (2) (2023) 341–351.
- [6] S. Zhang, D. Zfhaq, *Aerospace Materials Handbook*, CRC Press, Boca Raton, 2016.
- [7] I. Akande, O. Oluwole, O. Fayomi, O. Odunlami, Overview of mechanical, microstructural, oxidation properties and high-temperature applications of superalloys, *Mater. Today: Proc.* 43 (2) (2021) 2222–2231.
- [8] A. Pauzi, M. Ghazali, W. Zamri, A. Rajabi, Wear characteristics of superalloy and Hardface Coatings in gas turbine applications–A review, *Metals* 10 (9) (2020) 1171.
- [9] J. Chen, J. Chen, Q. Wang, Y. Wu, Q. Li, Ch Xiao, S. Li, Y. Wang, X. Hui, Enhanced creep resistance induced by minor Ti additions to a second generation nickel-based single crystal superalloy, *Acta Mater.* 232 (2022) 117938.
- [10] R. Darolia, Development of strong, oxidation and corrosion resistant nickel-based superalloys: critical review of challenges, progress and prospects, *Int. Mater. Rev.* 64 (6) (2019) 355–380.
- [11] A. Mouritz, *Introduction to Aerospace Materials*, Woodhead, 2012.
- [12] R. Reed, *Superalloys Applications*, Materials Technolology, 2007.
- [13] M. Koscakova, P. Korba, I. Sekelová, P. Koscak, D. Pastir, New trends in aviation development, in: *Analysis of Sustainable Aviation Fuels Market*, Nový Smokovec, 2022.
- [14] M. Klöwer, M. Allen, D. Lee, S. Proud, L. Gallagher, A. Skowron, Quantifying aviation's contribution to global warming, *Environ. Res. Lett.* 16 (10) (2021) 104027.
- [15] L. Xing, Y. Li, X. Chen, Status and role of the advanced composite materials in the development of aviation equipment, *Acta Mater. Compos. Sin.* 39 (9) (2022) 4179–4186.
- [16] V. Karbhari, Fabrication, quality and service-life issues for composites in civil engineering, in: *Durability of Composites for Civil Structural Applications*, Woodhead Publishing, 2007, pp. 13–30.
- [17] S. Aghniaie, S. Mohammad, S. Mahmoudi, Exergy analysis of a NovelAbsorption Refrigeration Cycle with expander and compressor, *Indian Journal ofScientific Research* 1 (2014) 815–822.
- [18] Y. Xu, J. Zhu, Z. Wu, Y. Cao, W. Zhang, A review on the design of laminated composite structures: constant and variable stiffness design and topology optimization, *Adv. Compos. Hybrid Mater.* 1 (2018) 460–477.
- [19] J. Zhu, H. Zhou, C. Wang, L. Zhou, S. Yuan, W. Zhang, A review of topology optimization for additive manufacturing: Status and challenges, *Chin. J. Aeronaut.* 34 (1) (2021) 91–110.
- [20] Y. Xiong, S. Yao, Z. Zhao, Y. Xie, A new approach to eliminating enclosed voids in topology optimization for additive manufacturing, *Addit. Manuf.* 32 (2020) 101006.
- [21] I.e. a. Ghionea, *Catia V5 Advanced Parametric and Hybrid 3D Design*, Routledge, 2022.
- [22] A.K. Kundu, *Aircraft Design*, Queen's University Belfast, Belfast, 2010.
- [23] T. Gowda, Optimization of design parameters of aircraft wing structure with Large Cut outs using Damage Tolerant design and finite element analysis approach, *Int. J. Recent Technol. Eng.* 8 (12) (2019).
- [24] H.N. Nabi, T. Lombaerts, Y. Zhang, E. van Kampen, Q. Chu, C.C. de Visser, Effects of structural failure on the safe flight envelope of aircraft, *J. Guid. Control Dynam.* 41 (6) (2018) 1257–1275.

- [25] P. Della Vecchia, Development of Methodologies for the Aerodynamic Design and Optimization of New Regional Turboprop Aircraft, Doctoral Thesis - University degli Studi di Napoli Federico II, 2013.
- [26] J. Ainsworth, C. Collier, P. Yarrington, R. Lucking, J. Locke, Aircraft Design Studies Based on the ATR 72, Society of Allied Weight Engineers, 2010.
- [27] European Aviation Safety Agency, Factor of Safety CS 25.303, EASA, 2015.
- [28] European Aviation Safety Agency, Limit Maneuvering Load Factors CS25.337, EASA, 2015.
- [29] P. Lancelot, Transonic flight and movable load modelling for wing-box preliminary sizing, 18th International Journal of Structural Integrity 8 (5) (2019).
- [30] J. Cutler, Understanding Aircraft Structures, Backwell Science, 2006.
- [31] F. Toffol, S. Ricci, A meta-model for composite wingbox sizing in aircraft conceptual design, Compos. Struct. 306 (2023) 116557.
- [32] Z. Wang, Z. Wan, R. Groh, X. Wang, Aeroelastic and local buckling optimisation of a variable-angle-tow composite wing-box structure, Compos. Struct. 258 (2021) 113201.
- [33] M. Picchi Scardaoni, M. Montemurro, E. Panettieri, Prandtlplane wing-box least-weight design: a multi-scale optimisation approach, Aero. Sci. Technol. 106 (2020) 106156.
- [34] D. Farrar, The Design of Compression Structures for Minimum Weight, Journal of the Royal Aeronautical Society, 1949.
- [35] D. Farrar, Investigation of Skin Buckling, Aeronautical Research Council Reports and Memoranda, 1953.
- [36] Castillo, M. Aceri, Highly orthotropic panels structural stability, Farrar and Bloch waves theory, International Journal of Structural Integrity 8 (5) (2017).
- [37] S. Zhang, D. Zhao, Aerospace Materials Handbook, CRC Press, 2016.
- [38] I. El-Sagheer, Finite element analysis of the behavior of bonded composite patches repair in aircraft structures, Frattura ed Intefrita Strutturale 14 (54) (2020) 128–138.
- [39] Z. Padovec, Experimental and numerical analyses of optimized composite profiles for aircraft construction, Mech. Compos. Mater. 58 (2) (2022) 283–292.
- [40] Avions de Transport Régional, ATR 72 Flight Manual, ATR Aircraft, 1989.
- [41] A. Castrichini, Preliminary investigation of use of flexible folding wing tips for static and dynamic load alleviation, Aeronaut. J. 121 (1235) (2016) 73–94.
- [42] V. Cusati, Development of a new methodology for the prediction of aircraft fuselage aerodynamic characteristics. Master thesis - Universita degli Studi di Napoli Federico II, 2013.
- [43] M.F. Nita, Aircraft Design Studies Based on the ATR 72, Project - Hamburg University of Applied Sciences, Hamburg, 2008.
- [44] T. Lisle, External spur gear root bending stress: a comparison of ISO 6336:2006, AGMA 2101-D04, Ansys Finite Element Analysis and strain gauge techniques, Mech. Mach. Theor. 111 (2017) 1–9.
- [45] M. Škorupa, Methodology for designing a system of Public Passenger transport in a functional region, Period. Polytech. Transp. Eng. 52 (1) (2024) 24–32.
- [46] P.C. Vijayan, S. Durairaj, Design and analysis of Passengner aircraft wing box, Int. J. Eng. Res. Technol. 7 (2) (2019).
- [47] E. Özbek, S. Ekici, T.H. Karakoc, Systems engineering approach on UAS, in: Unmanned Aerial Vehicle Design and Technology. Sustainable Aviation, Springer, 2023.
- [48] E. Gunaltili, S. Ekici, A. Kalkan, F.E. Gocmen, U. Kale, Z. Yilmazoglu, T.H. Karakoc, Conceptual Design and optimization of a sustainable and environmentally friendly archetypal helicopter within the selection criteria and limitations, Heliyon 9 (6) (2023).